Reprinted from: Transactions of the American Crystallographic Association, Vol. 5, pp. 113-131, 1969[*].

STRUCTURE DETERMINATION OF A FERROELECTRIC PHASE OF SODIUM NITRATE ABOVE 45 KBAR[†]

J. D. Barnett, J. Pack and H. T. Hall
Brigham Young University, Provo, Utah

ABSTRACT

The capability of the tetrahedral-anvil high-pressure X-ray diffraction apparatus to meaningfully measure line intensities is demonstrated by a study of $NaNO_3$ to 85 kbar. Anomalous line intensity changes near 45 kbar are shown to be due to a transition from R $\bar{3}$c space group to R3c with no measurable discontinuity in volume. The data suggest a higher-order transition in which the nitrate groups in alternate layers along the trigonal axis rotate in opposite directions under the influence of the pressure., and the nitrogen position is no longer planar with the oxygen atoms. The atomic configuration suggests a ferroelectric phase and dielectric measurements indicate a dielectric catastrophe at the transition point to give strength to the argument.

I. INTRODUCTION

As discussed extensively in another paper of this symposium,[1] in situ X-ray diffraction studies in the pressure range above ten kbar have been carried out using four general types of pressure-generating apparatus: (1) opposed diamond anvils[2,3] in which the X-ray beam traverses the sample in a direction parallel to the applied force on the diamond anvils, (2) opposed tungsten-carbide or diamond anvils[4,5,6,7] in which the X-ray beam traverses the sample in a direction perpendicular to the direction of the force applied to the anvils, (3) the tetrahedral-anvil apparatus[8] as described below, and (4) the split-belt apparatus.[9] With the notable exception of the work of Weir, Black and Piermarini,[10] all high-pressure in situ X-ray diffraction studies above ten kbar have been limited to the analysis of powder patterns. The pressure attainable using the first two techniques mentioned greatly exceed the maximum pressures reached in either the tetrahedral-anvil apparatus or the belt apparatus. The sample volume, however, is much smaller in the opposed anvil systems, and rather serious pressure gradients and flow patterns within the sample region exist. These gradients and resultant flow cause serious crystallite alignment which gives rise to preferred crystallite orientation. In the tetrahedral-anvil and belt apparatus, the geometry of the pressure chamber is such that gross pressure gradients are relatively far removed from the sample itself as are also any flow patterns.

The existence of preferred orientation and the associated inherent lack of reproducibility make impossible the quantitative analysis of X-ray intensity data to determine structural information. A survey of all published in situ data in this pressure range attests to these remarks since only line positions have been quantitatively utilized to characterize materials at high pressure. Intensity data, where reported, have been used only to support unit-cell dimensional analysis, and agreement is often notably poor. The work reported here represents the first analysis in which atomic positional parameters within the unit cell have been studied in situ using quantitative intensity measurements to distinguish the variations of these parameters with pressure.

---

[*] Proceedings of the Symposium on Crystal Structure at High Pressure at Pacific Science Center, Seattle, Washington, March 24, 1969. Available from Polycrystal book Service, P. O. Box 11567, Pittsburg, Pennsylvania 15238. Price $5.00

[†] This work was supported by the National Science Foundation and in part by the U. S. Army Research Office (Durham).

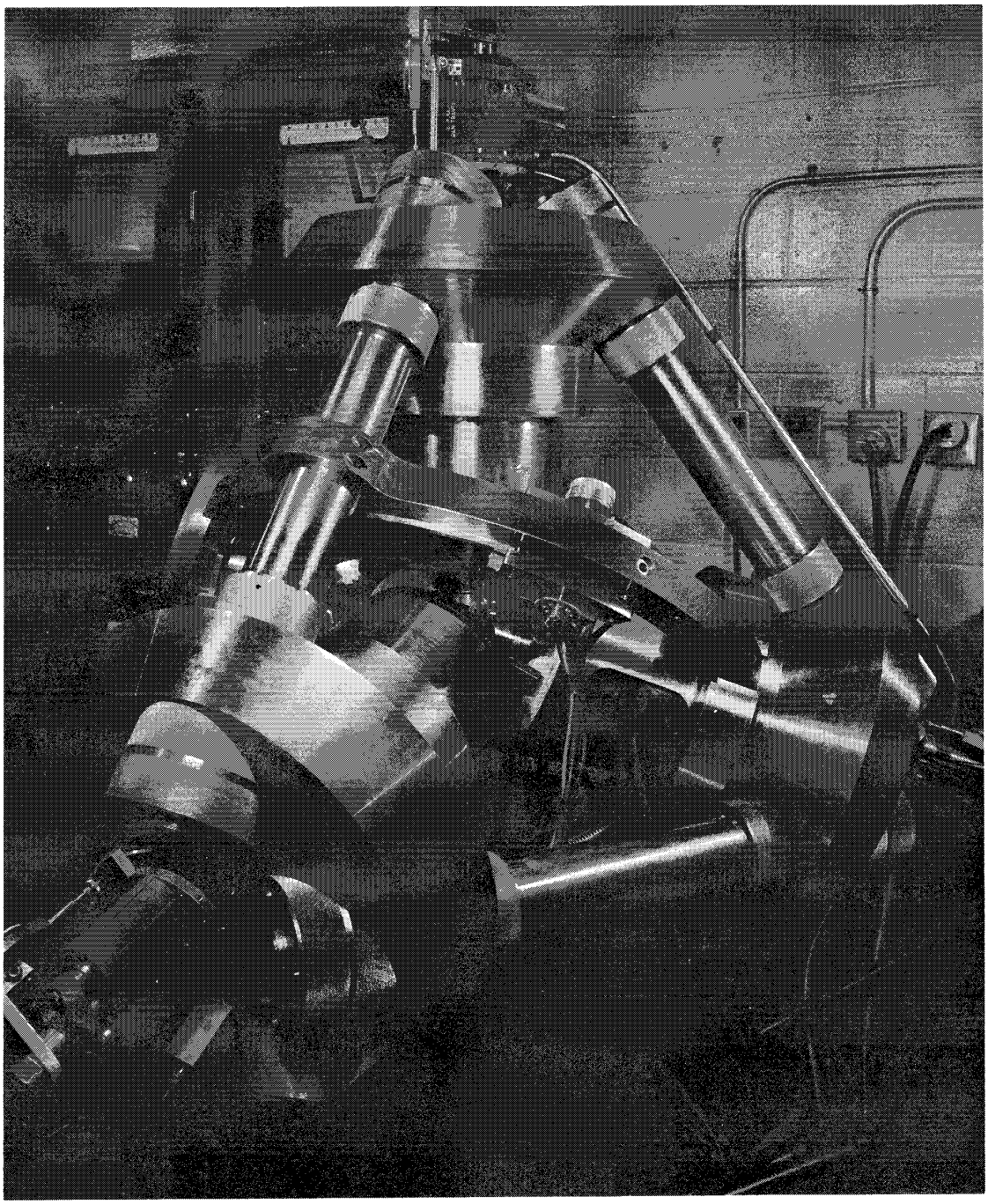

Fig. 1 Tetrahedral high-pressure, high-temperature X-ray diffraction apparatus.

The tetrahedral X-ray diffraction apparatus was used in this work. A photograph of the apparatus and a diagrammatic drawing showing the essential relationship of the X-ray geometry and the pressure system are shown in Fig. 1 and Fig. 2 respectively. A detailed discussion of the apparatus is found in a previous paper.[8] The system is basically a scanning diffractometer using scintillation counters with pulse-height discrimination to measure the X-ray powder pattern. Double-slit collimation is used on the entrance X-ray beams, and a double-slit collimation system is also placed in front of the counters as illustrated in Fig. 3. This collimation

on the counters is simply a background discrimination technique. Since the primary beam must pass through approximately three-fourths inch of pressure-supporting material in entering and leaving the sample chamber, an excessive amount of background scattered from this supporting material must be dealt with. The inclusion of the slits on the counter decreased the background by a factor of approximately 2.5. The use of the pulse-height selection further reduces the background by a factor of approximately 3. Two possible positions of the X-ray tube consistent with the high-pressure apparatus are indicated in Fig. 2, Fig. 3, and Fig. 4 and designated as geometry A and B as shown. Geometry B allows detection of a pattern on opposite sides of the direct beam and thus gives more precise angular data, and is used almost exclusively.

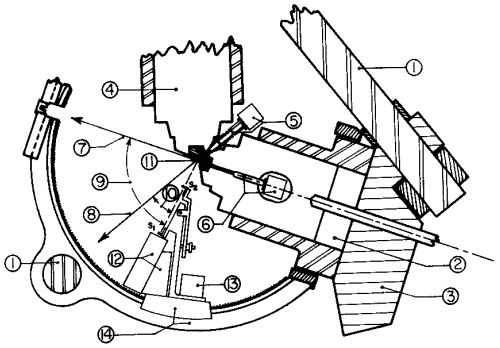

Fig. 2. Cross section of the apparatus showing the X-ray tube mounted in each position and the detector scanning mechanism as they relate to the high-pressure system. (1) tiebar, (2) hydraulic oil, (3) ram base, (4) piston assembly, (5) X-ray tube and collimator in position B, (6) X-ray tube and collimator in position A, (7) undeviated X-ray beam, position A, (8) undeviated X-ray beam, position B, (9) diffraction angle (2θ), position A, (10) diffraction angle (2θ) position B, (11) sample, (12) scintillation counter and pre-amp, (13) scanning motor, (14) scanning carriage and track.

The sample consists of a small flat disc pressed from 325-mesh powder of thickness made approximately equal to $1/\mu$ for maximum X-ray intensities using the transmission technique, where μ is the linear X-ray absorption coefficient of the sample material. The sample location and details of beam entrance and exit from the pressure chamber are shown in Fig. 4. The chamber material consists of low-z materials

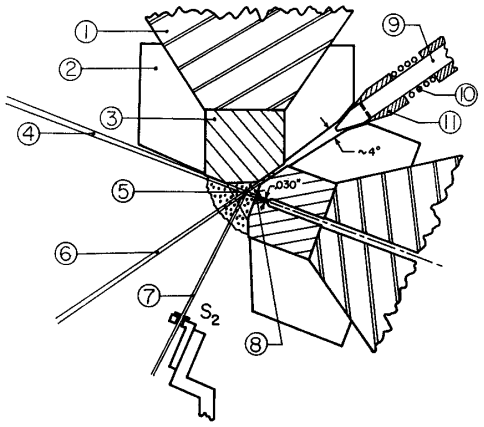

Fig. 3. Detail of the sample-chamber region and X-ray collimator for X-ray tube position B. Background discrimination by use of detector slit system is illustrated. (1) cemented tungsten-carbide anvil support, (2) steel anvil-binding ring, (3) carbide tetrahedral anvil, (4) region of undeviated X-ray beam, position A, (5) sample, (6) region of undeviated X-ray beam, position B, (7) region viewed by detector slits, (8) beryllium cone, (9) X-ray slit collimator, (10) spring, (11) collimator positioner.

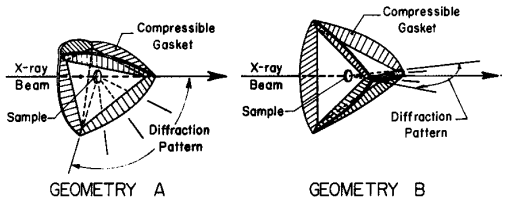

Fig. 4. Tetrahedral sample chamber showing the two possible X-ray geometries using the compressible gasket as the exit pupil.

such as LiH, B, and plastics. The most commonly used material is a boron-filled thermosetting phenolic plastic which also has temperature capabilities to approximately 1000°C at the higher pressures.

II. INITIAL X-RAY STUDY

Bridgman[11] reported a volume discontinuity of approximately 1.1 per cent in $NaNO_3$ at approximately 55 kbar. A rather routine attempt to determine the structure of the supposed high pressure phase yielded patterns which showed no

change in line positions, no new lines, and no lines disappearing as one traversed the pressure region specified by Bridgman. A rather marked and reversible change in line intensities was observed, however. The experiment was repeated with somewhat more care, and fourteen separate patterns covering the range from 8 to 85 kbar were obtained. Eight of these patterns are shown in Fig. 5 to indicate the quality of the patterns and the magnitudes of the intensity changes. Similar but less extensive sets of patterns have been obtained from five additional independent experiments, all of which showed repeatable and reversible intensity changes beginning at approximately 45 kbar. Pressure calibration was made by an independent X-ray experiment in which NaCl was mixed with $NaNO_3$, and lattice parameters measured to determine pressure from Decker's Equation of State.[12]

Experimental structure factors were reduced from the normalized intensities by dividing out the Lorentz-polarization and multiplicity factors and are found to vary smoothly with pressure. The ratio $F_{hkl}^2(P)/F_{hkl}^2(0)$ is given in Fig. 6a, where $F_{hkl}(P)$ represents the structure factor of the hkl line as a function of pressure. The anomalous spreading of these ratio curves at approximately 45 kbar is dramatic, to say the least. The fact that the intensity does not exhibit a discontinuity at this point but rather a discontinuity in slope is of special significance and suggests a higher order transformation rather than a first-order thermodynamic transformation. The reliability, or at least the reproducibility of intensity measurements in the tetrahedral-anvil X-ray diffraction apparatus is also indicated in Fig. 6a in the measurements below the transition point. The measured intensity ratios in this region appear to have a random uncertainty with a standard deviation of approximately five per cent. We have taken this value as an estimate of the measurement error in intensity determination.

Sodium nitrate has been extensively studied at atmospheric pressure at room temperature as well as at elevated temperature using single-crystal X-ray techniques.[13,14,15,16,17] The structure is rhombohedral with two formula units of $NaNO_3$ per unit cell. The space group is $R\,\bar{3}c$ with the nitrogen, sodium, and oxygen atoms in the special positions a, b, and e respectively and a position parameter x of the oxygen atoms when related to the hexagonal axis of 0.2448 ± 0.003 as given most recently by Cherin, Post,, and Hamilton.[12] This structure is shown in Fig. 7a and consists of layers of nitrate groups with alternate layers oriented 180° from each other.

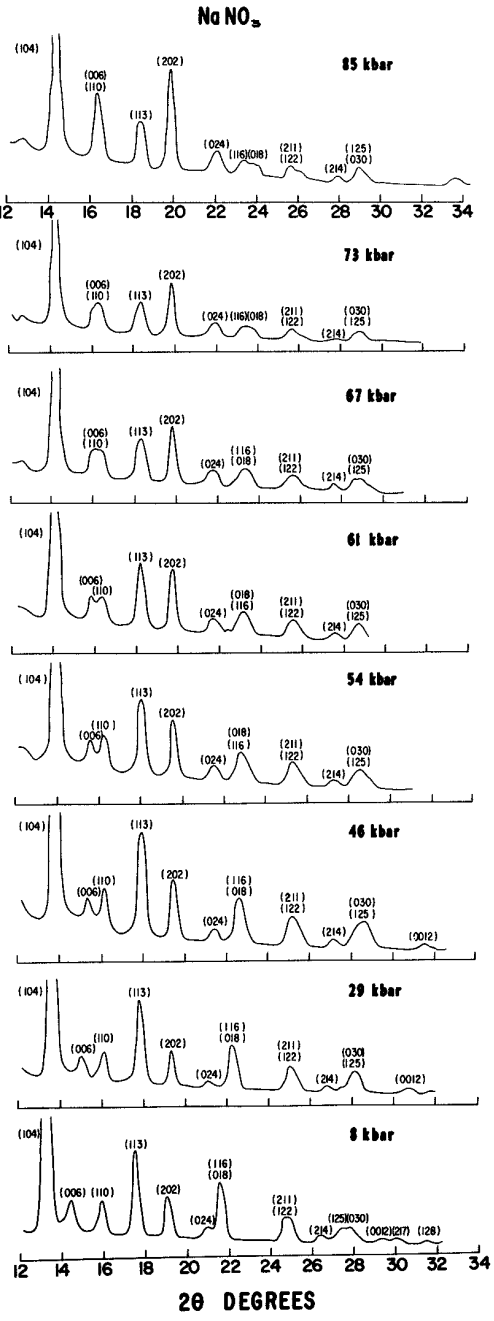

Fig. 5. Eight representative powder patterns of a series of 14 patterns recorded for $NaNO_3$ at room temperature between 8 kbar and 85 kbar. Indexing is in hexagonal system. Radiation is Mo Kα.

Sodium nitrate also exhibits a transformation at 275°C and atmospheric pressure. This transformation has been studied extensively[18,19,20] and shown to be an order-disorder transformation in which the nitrate group may have either the normal orientation or

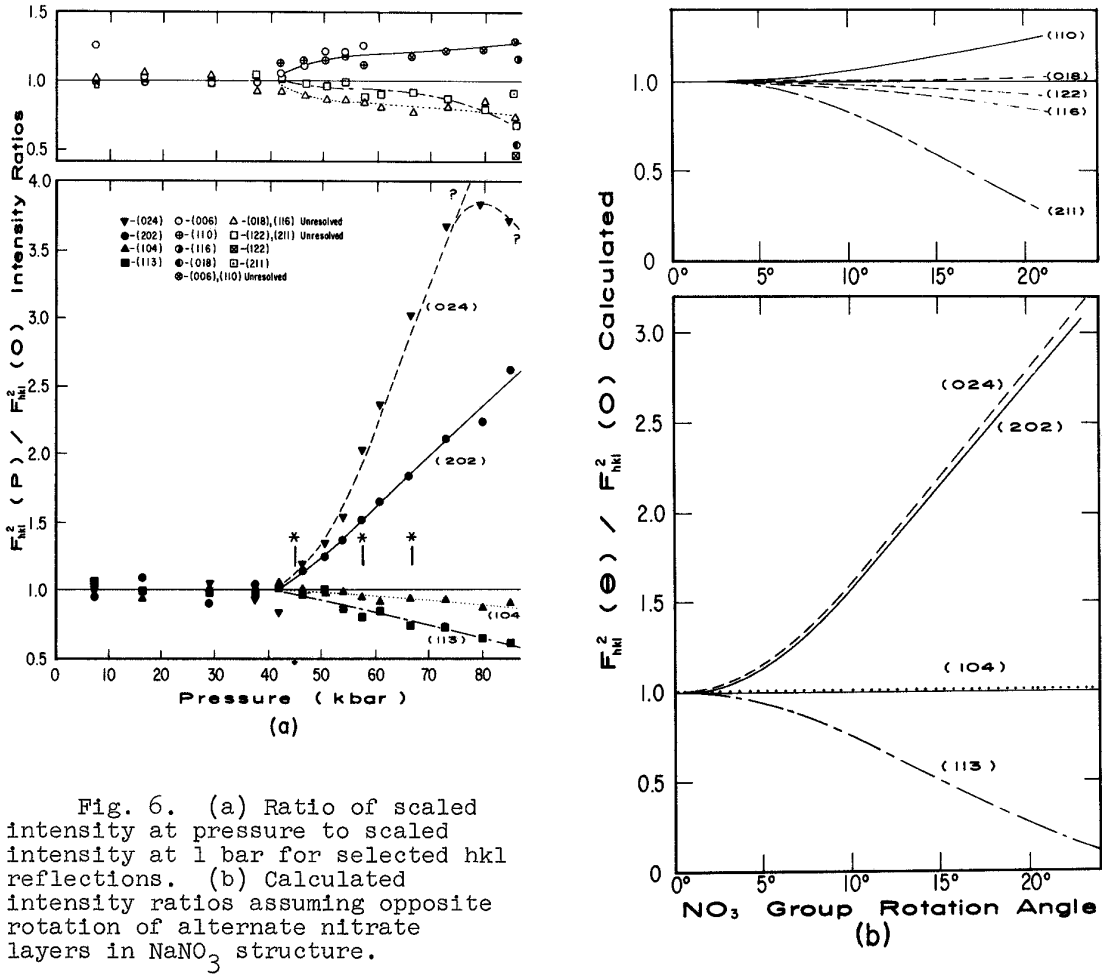

Fig. 6. (a) Ratio of scaled intensity at pressure to scaled intensity at 1 bar for selected hkl reflections. (b) Calculated intensity ratios assuming opposite rotation of alternate nitrate layers in $NaNO_3$ structure.

an orientation rotated 180°, and the probability of a particular group's being in one orientation or the other is random at temperatures above the transition. The phase line associated with this transformation has been studied by Rapoport[21] using DTA (differential thermal analysis) techniques and has been shown to increase in temperature with pressure as shown in Fig. 13 below, and is thus not directly related to this study. Measurements of anisotropic thermal factors at atmospheric pressure have indicated rather be an order-disorder transformation in which the nitrate group may have either the normal orientation or an anisotropic vibrational motion of the oxygen atoms but approximately isotropic motion of the Na and N atoms. In the analysis of the diffraction-line positions from the patterns of Fig. 5, all lines were indexed to a trigonal-rhombohedral unit cell both above and below the transition, and lattice constants were determined at each pressure. The results of this analysis are given as compressions in Fig. 8 along with calculated volumetric compressions. Within the sensitivity of the X-ray measurement, approximately 0.1 per cent in $\Delta a/a$ or $\Delta c/c$ and approximately 0.3 per cent in $\Delta V/V$, there appears to be no discontinuity in lattice constant or volume within the range of the experiment. This result contradicts the work of Bridgman[11] mentioned above but is consistent with the concept of a "higher-order" transition suggested by the X-ray intensity data.

Both the compression data and the X-ray intensity data suggest a transformation of a rather subtle nature in which only minor changes in atomic positions take place. Furthermore, as one approaches the transition from the high-pressure side, the high-pressure structure must approach the low-pressure structure according to the intensity data. Structure-factor calculations based on four simple models were carried out: (1) changes in the oxygen positional parameter x in R $\bar{3}$c, (2) movement of the Na and N along the c-axis, (3) rotation of all nitrate groups relative to the lattice, and (4) rotation of alternate layers of

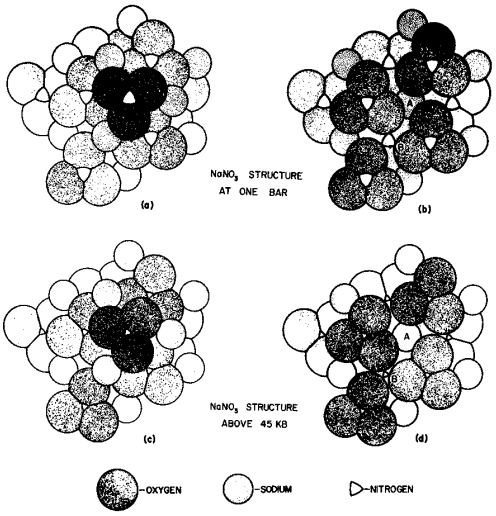

Fig. 7. (a) Pictorial view of $NaNO_3$ at one atmosphere looking along the trigonal c axis showing nitrate layers with orientation and position of nitrate groups with respect to the sodium atoms in R3c space group. (b) Same as (a) but with top nitrate group and three adjacent sodium atoms removed to illustrate similar voids below and above the nitrogen atom at points A and B respectively. (c) Proposed structure above 45 kbar in R3c space group with rotation angle of 15°. (d) Same as (c) but with top nitrate group and three adjacent sodium atoms removed to illustrate disimiliar voids below and above nitrogen atom at points A and B respectively as a result of the nitrate group rotation.

nitrate groups in opposite directions relative to the lattice. The calculated structure factors from the first three models were obviously not appropriate fits since neither magnitudes nor even the sign of the calculated variations agreed with Fig. 6a. The results of the fourth calculation are given in Fig. 6b. Although quantitative agreement leaves something to be desired, the qualitative agreement is obvious, and indicated the direction for further investigation. Note that the magnitude of the rotations involved is rather large and impressive.

Such alternate rotation destroys all point-inversion symmetries, as well as all rotation and screw axes perpendicular to the c-axis. The resulting space group is R3c. The positions formerly occupied by the Na and N atoms are no longer special positions along the c-axis in the new space group, and thus by symmetry argument they should be allowed to move in the calculations. In the patterns shown in Fig. 5, only eight to ten lines were well-resolved, and $NaNO_3$

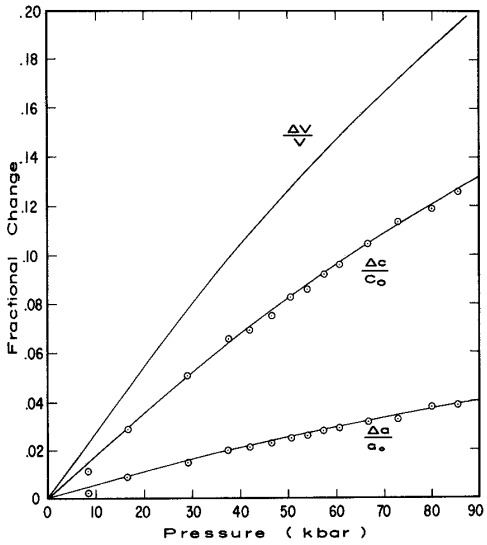

Fig. 8. Lattice and volume compression for $NaNO_3$ to 85 kbar as determined from X-ray measurements.

in the R3c space group requires a minimum of four positional parameters and one scale factor. This condition makes the meaning of any least-square fitting procedure very dubious. Further analysis of this data was therefore not undertaken.

III. IMPROVED X-RAY DATA AND FITTING IN THE R3c SPACE GROUP

Three additional patterns with slightly improved resolution were taken at pressures of 45 kbar, 58 kbar, and 67 kbar as indicated by lines and asterisk (*) in Fig. 6a. Peaks from these patterns were computer fitted to gaussian curves in order to separate doublets and triplets. This procedure yielded 24, 22, and 21 measurable intensities for the three pressures respectively.

Data from each of these three patterns were least-square fitted by calculation using the Oak Ridge Fortran Least Squares (ORFLS) program with the Na and N atoms each in special position a and the oxygen atoms in special position b. The origin was taken relative to the hexagonal axis such that at pressures below the transition the N positions would be (0, 0, 0) and (0, 0, ½) and above the transition would be (0, 0, Z_N) and (0, 0, ½ + Z_N) and translated consistent with the rhombohedral symmetry. The Na position would be (0, 0, ¼) and (0, 0, ¾) below the transition and (0, 0, Z_{Na}) and (0, 0, ½ + Z_{Na}) above the transition. The oxygen positions below

the transition are then (x, 0, 0) (0, x, 0) ($\bar{x}$, $\bar{x}$, 0) ($\bar{x}$, 0, ½) (0, $\bar{x}$, ½) (x, x, ½) and above the transition at (x, y, 0) (y, x-y, 0) ($\bar{y}$, $\bar{x}$, ½) (x, x-y, ½) (y-x, y, ½). As a check on the model and the meaningfulness of particular parameter changes, several least-squares. calculations were made holding different combinations of parameters fixed. The results of these calculations are shown in Table I. Atomic scattering factors were taken from the International Tables for X-ray Crystallography[22] using $0^{-2/3}$, N^{+l}, and Na^{+l} valence states. Isotropic thermal parameters for nitrogen, sodium, and anisotropic thermal parameters for oxygen were taken from the work of Cherin et al.[13] at zero pressure and were inserted into the program but were not varied except as discussed below. In Table I those parameters which were held fixed are placed in brackets [ ]. After the analysis was completed using fixed thermal parameters, a few calculations were made in which the anisotropic thermal parameter β_{33} of Na and N was allowed to vary, and the results are also shown in Table I. The error estimates are taken directly from the output of the ORFLS program. The computer was programmed to refine on F^2 values, and the R factors recorded in Table I were obtained from

$$R = \frac{\Sigma W\left[F_0^{\,2} - F_c^{\,2}\right]^2}{\Sigma W\left(F_0^{\,2}\right)^2}$$

using unit weights. Since the motion of the oxygen atoms is basically a rotation about the symmetry axis, positional parameters, Θ_0 and u_0, in a polar coordinate notation are also shown in Table I where u_0 is the fractional radial distance of the oxygen atoms from the symmetry axis. The parameter u_0 is thus related to the O-N bondlength, which is equal to u_0 multiplied by the lattice constant a. In the last column of Table I is given an indication of the significance level associated with the parameters varied in the calculation. This column follows the procedures set forth by Hamilton[23] in his $\mathfrak{R}$-ratio test of significance in which a least-square structural fit with a set number of variable parameters is compared with a similar calculation with a restricted number of parameters to test the significance of the "freed" parameters in the structure. For example, Trial 6 on the 57 kbar data includes Z_{Na} which is restricted in Trial 4 to a fixed value. The significance level of .005(confidence interval of 99.5%) implies that the Z_{Na} variable is required to describe the structure.

When using fixed thermal factors, the most meaningful least-square fit based upon Hamilton's criteria is shown in Table I for each of the three pressures by an asterisk (*). These results as a function of pressure are then shown in graphical form in Figs. 9a, b, c, and d. The solid straight lines are required by the symmetry. The dotted curves are simply drawn through the three measured points. The error flags are those taken from the output of the ORFLS program.

The dotted curves for the parameters Θ_0 and Z_{Na} are drawn such as to approach the low-pressure modification rather than exhibit a discontinuity. This conclusion is based largely upon the more extensive but less precise data shown in Fig. 6a and the rather close correspondence with Fig. 6b in the region near the transition point. This interpretation is of course subject to question; a proof of the lack of a discontinuity is not easy, and the existence of a discontinuity is undetectable unless the discontinuity is large compared to the measuring sensitivity. As indicated by the error flags associated with the determination of Z_N and u_0, these values are less well-defined and require further study.

Some features of the high-pressure structure can be visualized in a simple manner by considering only the nitrate groups and sodium atoms which lie along the trigonal axis of the rhombohedral cell. Such a diagram is shown in Fig. 10a for $NaNO_3$ below the transition in the R $\bar{3}$c symmetry and in Figs. 10b and 10c for two equivalent arrangements in the R3c symmetry which exhibit reversed orientation as a result of an exchange of rotation direction in alternate nitrate layers. The movement of the sodium and nitrogen atoms along the trigonal axis has been exaggerated for emphasis. The polar nature of the structure in the R3c space group is very evident as illustrated by Figs. 10b and 10c.

As a further elucidation of the structure the drawings of Figs. 7b, 7c and 7d were made where the structure is viewed in the direction of the c-axis. Fig. 7c shows the structure above the transition pressure with the alternate layer rotation angle Θ_0 of 15°. Figs. 7b and 7d are identical to Figs. 7a and 7c respectively but with the top nitrate group and three sodium atoms removed in order to see the region below the nitrate group and the Na ion. It is evident that the rotation of the nitrate group creates a relatively large void in the region A immediately below the nitrogen and above the sodium atoms. The

Table I

Results of least-squares trial refinements on the three sets of data in which different parameters are allowed to vary to determine significance of particular parameters in the model used to describe $NaNO_3$ at high pressure.

	Trial	STRUCTURE PARAMETERS							R	No. of Variables	Significance Level[a]
		x_0	y_0	θ_0	u_0	Z_{Na}	Z_N	β_{33N}			
45 Kbar (24 Peaks)	1	.241 ± .005	[0]	[0]	.2410 ± .005	[.25]	[.50]	[.0009]	.146	2	-------
	2	.255 ± .008	.027 ± .012	5.5° ± 2.4°	.2426 ± .008	[.25]	[.50]	[.0009]	.142	3	< .25 rel. to tr. 1[b]
	3	.241 ± .005	[0]	[0]	.2410 ± .005	[.25]	.488 ± .004	[.0009]	.138	3	< .10 rel. to tr. 1
	4*	.256 ± .007	.029 ± .010	5.9° ± 2.6°	.2426 ± .007	[.25]	.487 ± .004	[.0009]	.129	4	< .10 rel. to tr. 1
	5	.255 ± .007	.027 ± .011	5.5° ± 2.2°	.2426 ± .007	[.25]	[.50]	.0052 ± .0025	.130	4	< .10 rel. to tr. 1
	6	.254 ± .008	.027 ± .012	5.6° ± 2.5°	.2416 ± .008	.253 ± .006	[.50]	[.0009]	.141	4	> .5 rel. to tr. 2
	7	.255 ± .007	.026 ± .010	5.3° ± 2.0°	.2428 ± .007	.250 ± .005	.485 ± .004	[.0009]	.129	5	> .5 rel. to tr. 4
	8	.256 ± .007	.029 ± .010	5.9° ± 2.0°	.2426 ± .007	.252 ± .004	[.50]	.0056 ± .0026	.129	5	> .5 rel. to tr. 5
57 Kbar (22 Peaks)	1	.246 ± .009	[0]	[0]	.2460 ± .009	[.25]	[.50]	[.0009]	.237	2	--------
	2	.279 ± .009	.060 ± .010	11.8° ± 2.0°	.2543 ± .009	[.25]	[.50]	[.0009]	.189	3	< .005 rel. to tr. 1
	3	.247 ± .008	[0]	[0]	.2470 ± .008	[.25]	.480 ± .005	[.0009]	.213	3	< .05 rel. to tr. 1
	4	.278 ± .008	.056 ± .008	11.0° ± 1.6°	.2545 ± .008	[.25]	.482 ± .004	[.0009]	.162	4	< .025 rel. to tr. 2
	5	.279 ± .007	.058 ± .008	11.4° ± 1.6°	.2549 ± .007	[.25]	[.50]	.008 ± .004	.159	4	< .025 rel. to tr. 2
	6*	.272 ± .006	.052 ± .006	10.4° ± 1.2°	.2500 ± .006	.261 ± .002	.489 ± .004	[.0009]	.124	5	< .005 rel. to tr. 4
	7	.278 ± .007	.057 ± .008	11.2° ± 1.6°	.2541 ± .007	[.25]	.521 ± .005	.0004 ± .0047	.155	5	< .025 rel. to tr. 2
	8**	.271 ± .005	.049 ± .005	9.8° ± 1.0°	.2501 ± .005	.2634 ± .0017	.503 ± .007	.0100 ± 0036	.103	6	< .01 rel. to tr. 6
68 Kbar (21 Peaks)	1	.250 ± .010	[0]	[0]	.2500 ± .010	[.25]	[.50]	[.0009]	.385	2	---------
	2	.291 ± .010	.073 ± .009	14.0° ± 1.7°	.2621 ± .010	[.25]	[.50]	[.0009]	.284	3	< .005 rel. to tr. 1
	3	.292 ± .011	.072 ± .010	13.7° ± 1.9°	.2632 ± .011	[.25]	.482 ± .005	[.0009]	.277	4	< .50 rel. to tr. 2
	4	.283 ± .005	.067 ± .005	13.1° ± 1.0°	.2559 ± .005	.2684 ± .0012	[.50]	[.0009]	.143	4	< .005 rel. to tr. 2
	5*	.284 ± .005	.068 ± .004	13.3° ± .8°	.2567 ± .004	.2658 ± .0014	.491 ± .003	[.0009]	.129	5	< .10 rel. to tr. 4
	6	.282 ± .004	.065 ± .004	12.7° ± .8°	.2557 ± .004	.2681 ± .0011	[.50]	.0096 ± .004	.118	5	< .025 rel. to tr. 4
	7**	.282 ± .004	.065 ± .004	12.7° ± .8°	.2557 ± .004	.2680 ± .0014	.498 ± .005	.0090 ± .004	.117	6	> .5 rel. to tr. 6
	8+	.282 ± .004	.065 ± .004	12.7° ± .8°	.2557 ± .004	.2676 ± .0015	[.50]	.0094 ± .004	.117	6	> .5 rel. to tr. 6

* Most significant fit without using variable thermal parameters.

** Most significant fit using variable thermal parameters.

a Following procedure of Hamilton (Ref. 24)

b <.005 Relative to Trial 1

\+ β_{33Na} allowed to vary

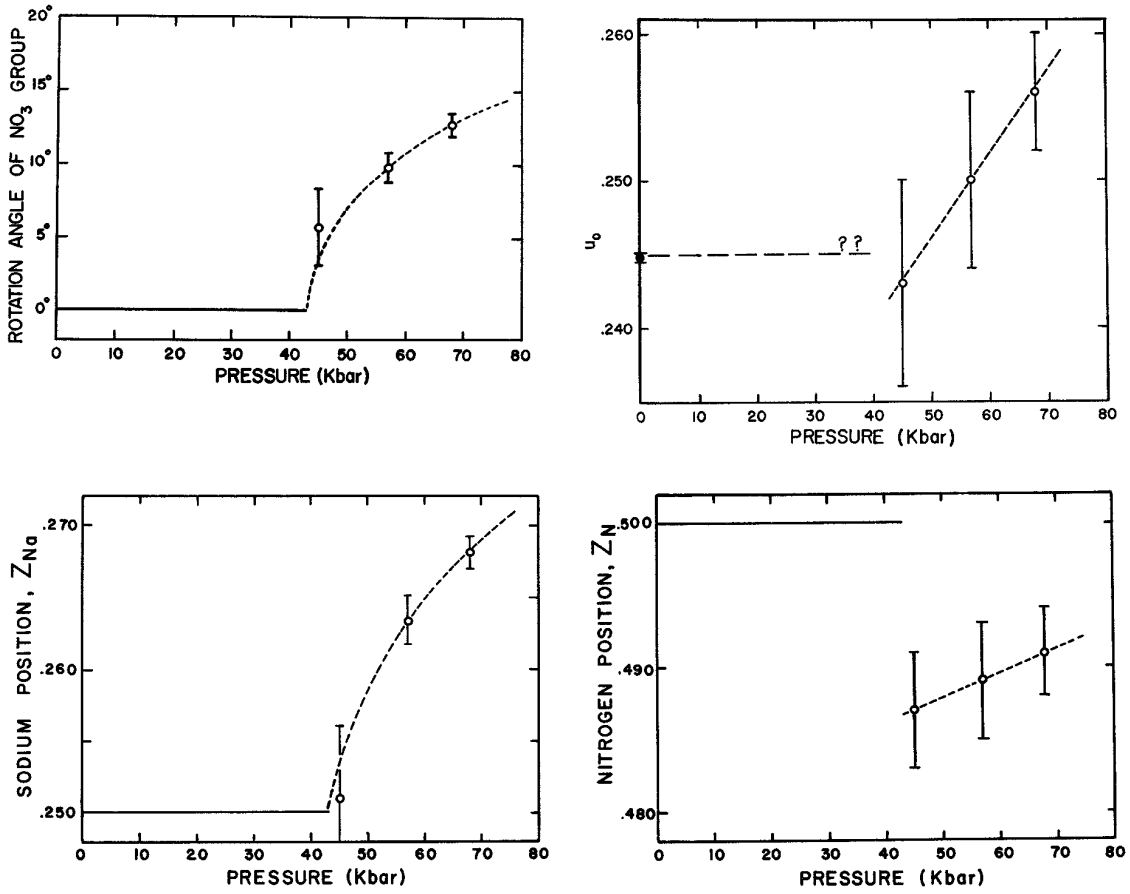

Fig. 9. Result of calculated least-squares refinements showing positional parameters as a function of pressure when thermal parameters were not allowed to vary. Solid lines represent positions restricted by $R\bar{3}c$ symmetry below the transition. (a) Magnitude of opposite rotation of nitrate groups in alternate layers; (b) radial positional parameter for oxygen from trigonal axis; (c) positional parameter for sodium along trigonal axis; (d) positional parameter for nitrogen along trigonal axis.

decrease in the size of the void above the nitrogen and below the sodium in the region B is also apparent. Figs. 7c and 7d correspond to Fig. 10b when viewing Fig. 10b from the top. The size of the voids suggested by Fig. 7 indicates the movement of the sodium up along the c-axis and the movement of the nitrogen down in accordance with the data discussed above. This pictorial argument simply points out that the rotation of the nitrate groups, the motion of the sodium, and the less well-defined motion of the nitrogen atom in the direction previously described are all self-consistent and part of a common movement in the crystal.

The existence of these rather large voids in the vicinity of the sodium and nitrogen atoms suggested the possibility of rather large anisotropy in the thermal parameters associated with these two atoms and in particular with the nitrogen atom. As indicated in Table I, several least-squares-fit calculations were made in which only the thermal parameter β_{33} for nitrogen was allowed to vary. The results of these calculations indicate a much higher thermal vibration of the nitrogen atoms along the c-axis at high pressures than at atmospheric pressures. Furthermore, the X-ray intensity data cannot distinguish between vibrational motion of the nitrogen and a change in positional parameter in the direction indicated above. This feature of the analysis throws serious

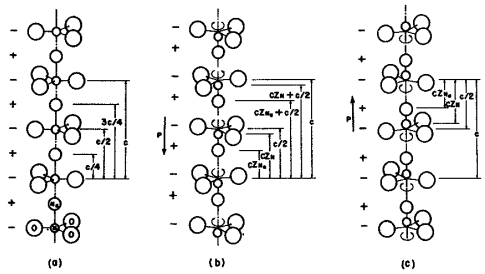

Fig. 10. Atomic arrangements along the trigonal axis showing symmetry below transition in (a) and the break in symmetry and resultant creation of electric dipoles above transition in (b) and (c). The symmetry break also gives rise to two possible polar orientations and suggests possible ferroelectric domain structure.

doubt into the validity of the results for the nitrogen positional parameters shown in Fig. 9d and gives added strength to the concept of a higher-order transformation across which no positional parameter discontinuity can occur. The vibrational feature does imply the intimate involvement of the nitrogen atom in the transformations. Three trial calculations were also made in which both Z_N and β_{33N} were simultaneously varied but the computer failed to converge in each case. Only one least-squares fit was made in which the anisotropic thermal parameter β33 for Na was allowed to vary. This was trial eight at 68 kbar in Table I. The results yielded very little change in other parameters, and the resultant vibrational amplitude of the Na atom was only slightly larger in the c-direction than given by Cherin, et al. at zero pressure. The need for a greater number of line intensities and more data both below and above the transition to further clarify the role of the nitrogen atom in the transformation mechanism is obvious.

IV. DIELECTRIC MEASUREMENTS

The non-centro symmetric, polar nature of $NaNO_3$ in the R3c space group is apparent from an elementary look at the electrical charge distribution in Figs. 10b and 10c. This charge distribution suggests very strongly that $NaNO_3$ is ferroelectric at pressure above the transition at 43 kbar. Based upon the X-ray diffraction evidence, a parallel-plate capacitor consisting of ten pressed-powder $NaNO_3$ discs 0.250 inch in diameter by 0.010 inch thick alternated with aluminum conducting foils was constructed. This

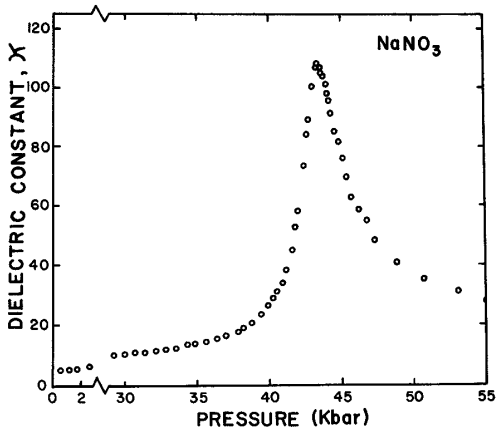

Fig. 11. Dielectric constant measurements as a function of pressure showing dielectric catastrophe at transition point.

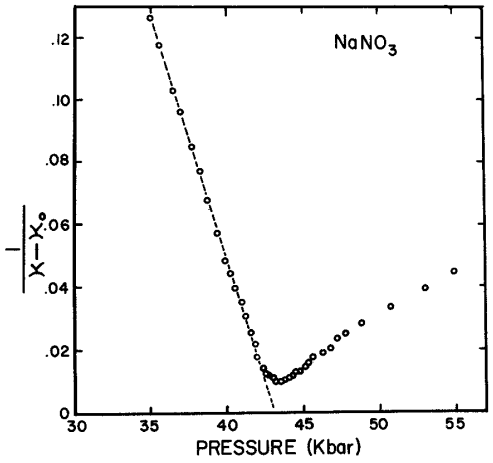

Fig. 12. Reciprocal dielectric constant as a function of pressure indicating agreement with a Curie-Weiss type variation.

capacitor was subjected to a pressure of 55 kbar in a six-anvil cubic press to measure the in situ dielectric constant of the material. Results of the experiment, which was repeated twice, is shown in Fig. 11. The existence of a dielectric catastrophe in the region of the transition point is obvious and gives strength to the hypothesis that the high-pressure phase of $NaNO_3$ is ferroelectric. The polar nature of the structure shown in Fig. 10 also suggests the two possible ferroelectric domain orientations and possible growth mechanisms. Work is currently in progress to measure a spontaneous polarization under pressure on oriented single-crystal samples

and thus to give complete confirmation of the hypothesis.

If one assumes that the high-pressure phase is ferroelectric, several interesting interpretations are possible which, due to their consistency with the X-ray data, give further strength to the hypothesis. The dielectric catastrophe associated with a ferroelectric transition generally exhibits a Curie-Weiss variation of dielectric constant K with temperature; that is, $K = C/(T - T_0)$ where C is known as the Curie-Weiss constant and T_0 is the Curie temperature. If the phase line on the PT diagram is assumed linear over a limited region, the Curie-Weiss relationship gives rise to a variation of the dielectric constant with pressure similar to the Curie-Weiss relationship itself; that is, $K = C/(P - P_0)$ where P_0 is the transition pressure. Such an equation will be true only for that contribution to the dielectric constant associated with the dielectric catastrophe, however. A plot of P vs $1/(K - K_0)$ where K_0 is the zero-pressure dielectric constant is shown in Fig. 12 and demonstrates the essential agreement with a Curie-Weiss type law below the transition pressure and the qualitative agreement above this pressure. The lack of a discontinuity in the dielectric constant as one traverses the transition is significant and is typical of a second-order ferroelectric transition when studied as a function of temperature. This fact is in substantial agreement with the previous X-ray arguments for a thermodynamic higher-order transformation.

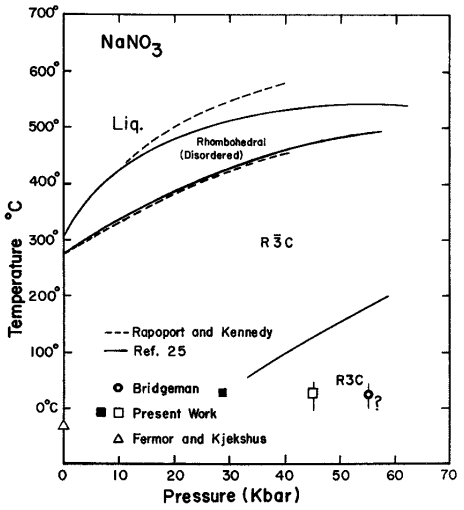

Fig. 13. Phase diagram of $NaNO_3$ indicating various unexplained phenomena in the high-pressure moderate-temperature region.

As a final point of interest, one should note that current mechanistic theories for ferroelectric transitions are based upon the existence of a particular vibrational mode of the crystal which has a critically high amplitude and attendant low spring constants at the transition. The low spring constant gives rise to high dielectric polarizability and the resultant high dielectric constant. The unusually high vibrational amplitude of the nitrogen atom experimentally indicated, but not proven, from the X-ray data for $NaNO_3$ above 45 kbar may well be associated with this mechanism.

Other studies which have recently been carried out on $NaNO_3$ by other workers as well as this work attest to the fact that $NaNO_3$ exhibits numerous anomalies which are currently not understood. A phase diagram showing the location in PV space where anomalous behavior has been observed is shown in Fig. 13. The phase line of the order-disorder transition referred to above, which occurs at 275°C atatmospheric pressure, was studied both by Rapoport[21] and by a group at General Dynamics.[24] The General Dynamics group also indicated the existence of a phase line at higher pressures and lower temperatures as shown in Fig. 13. This line was detected using a "differential thermal conductivity analysis" (DTCA) technique. In conjunction with the dielectric measurements reported herein, an electrical resistance measurement indicated a resistance anomaly at 29 kbar and room temperature in good agreement with the General Dynamics group. Neither of these agree with the dielectric catastrophe and the associated structural change at room temperature and 43 kbar which is the main thesis of this paper. Fermor and Kjekshus[20] have recently reported a small dielectric anomaly at atmospheric pressure and -30°C to complicate the diagram.

V. CONCLUSIONS

The data presented above demonstrate with little reservation the ability of the Tetrahedral-Anvil X-ray apparatus to obtain high-pressure in situ X-ray powder data which can meaningfully be used to determine structure information on simple systems involving a limited number of positional parameters.

Although the evidence is not conclusive without spontaneous polarization measurements, the consistency of the X-ray analysis and the dielectric measurements give very strong indications of the existence of a high-pressure

ferroelectric modification of $NaNO_3$. The complexity of the $NaNO_3$ phase diagram as presently understood suggests the need for further work to elucidate the anomalous behavior in the high-pressure, moderate temperature range and the determination of the phase lines associated with these anomalous effects. This report is to be considered a progress report on $NaNO_3$ since further X-ray analysis as well as dielectric measurements are in progress, and will be reported in a latter publication along with the detailed tables of calculated structure factors.

The authors acknowledge the aid of R. B. Bennion who carried out some of the original measurements, C. Candland who helped with some of the original analysis, and to L. Merrill for assistance in some of the computer programs and for helpful discussions.

NOTE ADDED IN PROOF:

Experimental observation of dielectric hysterisis on $NaNO_3$ above 45 kbars, made since the presentation, has confirmed the ferroelectric nature of the high pressure phase.

[1] D. B. McWhan, Trans. Amer. Cryst. Assoc. **5**, 39 (1969).
[2] G. J. Piermarini and C. E. Weir, J. Res. Natl. Bur. Std., **66A**, 325 (1962).
[3] W. A. Bassett, T. Takahashi, and P. W. Stook, Rev. Sci. Instr., **38**, 37 (1967).
[4] E. A. Perez-Albuerne, K. F. Forsgren, and H. G. Drickamer, Rev. Sci. Instr., **35**, 29 (1964).
[5] J. C. Jamieson and A. W. Lawson, J. Appl. Phys., **33**, 776 (1962).
[6] D. B. McWhan and W. L. Bond, Rev. Sci. Instr., **35**, 626 (1964).
[7] N. B. Owen, et al., J. Phys. Chem. Solids, **24**, 1519 (1963).
[8] J. D. Barnett and H. T. Hall, Rev. Sci. Instr., **35**, 175 (1964).
[9] P. J. Freud and C. B. Sclar, "Symposium on the Accurate Characterization of the High-Pressure Environment," U. S. Dept. of Commerce, National Bureau of Standards, Gaithersburg, Maryland. Oct. 14-18, 1968.
[10] C. Weir, S. Block and G. Piermarini, J. Natl. Bur. Std., **69C**, 275 (1965).
[11] P. W. Bridgman, Proc. Am. Acad. Sci., **76**, 1 (1945).
[12] D. L. Decker, J. Appl. Phys., **36**, 157 (1965).
[13] P. Cherin, W. C. Hamilton and B. Post, Acta. Cryst., **23**, 455 (1967).
[14] E. Kurki-Suonio, Ann. Acad. Sci. Fennicae, Series A, **84**, 1 (1962).
[15] 0. Inkinen, Ann. Acad. Sci. Fennicae, Series A, **55**, 1 (1960).
[16] R. L. Sass, R. Vidale and J. Donohue, Acta. Cryst., **10**, 567 (1957).
[17] P. E. Tahvonen, Ann. Acad. Sci. Fennicae., Series A, **42**, 1 (1947).
[18] J. A. A. Ketelaar and B. Strijk, Recl. Trav. Chim. Pays-Bas. Belg., **645,** 174 (1945).
[19] L. A. Siegel, J. Chem. Phys., **72**, 1146 (1949).
[20] J. H. Fermor and A. Kjekshus, Acta. Chem. Scand., **22**, 1628 (1968)
[21] E. Rapoport., J. Phys. Chem. Solids, **27**, 1349 (1966).
[22] International Tables for X-ray Crystallography, Vol. III, p. 218, Birmingham: Kynoch Press.
[23] W. C. Hamilton, Acta Cryst., **18**, 502 (1965).
[24] Fort Worth Division of General Dynamics, Research Summary, Applied Research Program, January-June 1966, ARR-10 p. 84.